

Thermodynamic and electrical transport properties of UTe_2 under uniaxial stressClément Girod ^{1,*}, Callum R. Stevens ², Andrew Huxley ², Eric D. Bauer ¹, Frederico B. Santos ¹, Joe D. Thompson ¹, Rafael M. Fernandes ³, Jian-Xin Zhu ¹, Filip Ronning ¹, Priscila F. S. Rosa ¹ and Sean M. Thomas ^{1,†}¹*Los Alamos National Laboratory, Los Alamos, New Mexico 87545, USA*²*School of Physics and Astronomy and Centre for Science at Extreme Conditions, University of Edinburgh, Edinburgh EH9 3FD, United Kingdom*³*School of Physics and Astronomy, University of Minnesota, Minneapolis, Minnesota 55455, USA*

(Received 25 May 2022; accepted 26 July 2022; published 1 September 2022)

Despite intense experimental efforts, the nature of the unconventional superconducting order parameter of UTe_2 remains elusive. This puzzle stems from reports of either a single or a double superconducting transition at ambient pressure as well as a complex pressure-temperature phase diagram. To address this issue, we measured the heat capacity and electrical resistivity of UTe_2 under compressive uniaxial stress σ applied along different crystallographic directions. We find that the critical temperature T_c of the single observed bulk superconducting transition decreases with σ along [100] and [110] but increases with σ along [001]. Aside from its effect on T_c , c -axis stress leads to a significant piezoresistivity. Importantly, an in-plane shear stress σ_{xy} does not induce any observable splitting of the superconducting transition over a stress range of $\sigma_{xy} \approx 0.17$ GPa. This result suggests that the superconducting order parameter of UTe_2 may be single component at ambient pressure.

DOI: [10.1103/PhysRevB.106.L121101](https://doi.org/10.1103/PhysRevB.106.L121101)

Unconventional superconductor UTe_2 is a promising candidate for spin-triplet pairing and topological superconductivity [1]. Yet, despite intense experimental efforts (see Ref. [2]), the nature of the superconducting order parameter (OP) of UTe_2 remains elusive. UTe_2 is believed to host multiple superconducting phases as a function of hydrostatic pressure [3–7] and magnetic field [5–9], but the number of superconducting transitions at ambient conditions is a matter of contention [2].

At zero field and ambient pressure, several studies suggest that UTe_2 is a chiral superconductor based on the observation of chiral surface states [10,11], a gap structure with point nodes [12], and a broken time reversal symmetry (TRS) in the superconducting state [13,14]. Due to the presence of two distinct thermodynamic superconducting anomalies in some samples [13], UTe_2 is proposed to possess two superconducting OPs. Additionally, the trainability of the polar Kerr signal with magnetic field along the crystallographic c axis suggests that the product of these two superconducting OPs transforms as the B_{1g} irreducible representation (irrep) of the orthorhombic point group D_{2h} [13,14]. Importantly, because this point group has no multidimensional irreps, a description in terms of a two-component gap necessarily requires nearly or accidentally degenerate superconducting instabilities.

Although some samples display two features in the specific heat across the superconducting transition, UTe_2 crystals that display an optimal superconducting transition temperature $T_c = 2$ K and large residual resistivity ratios host a single thermodynamic superconducting transition, as manifested by a single jump in the specific heat [15,16]. This could be

either an indication that the two OPs condense at very similar temperatures that cannot be resolved in the specific heat or that higher T_c samples display only one superconducting OP. Reports of broken TRS in the superconducting phase of single-transition samples are lacking, and therefore the nature of the superconducting OP is still unclear.

In samples with a single superconducting transition (i.e., one jump in the specific heat), pressure splits the transition into two thermodynamic anomalies that have an opposite pressure dependence above 0.3 GPa [3]. For samples with two peaks in the specific heat at ambient pressure, four peaks are observed above 0.3 GPa [4]. Upon further increasing pressure, an antiferromagnetic phase is argued to emerge [3,4], in contrast with the ferromagnetic fluctuations initially expected at ambient pressure [1,17]. The connection between pressure-induced magnetic fluctuations and the splitting of the superconducting transitions at low pressure remains unclear [18].

Uniaxial stress has proved to be a powerful tool to study multicomponent superconductors. This technique has been used extensively to study the phase diagram and the OP of Sr_2RuO_4 [19,20]. While this material was initially thought to display spin-triplet pairing [21], recent NMR data performed under strain demonstrated it to be actually a singlet superconductor [22].

Here, we investigate the nature of the superconducting OP of UTe_2 by measuring the low-temperature ac heat capacity and the electrical resistivity of single crystals under compressive uniaxial stress σ_{100} , σ_{110} , and σ_{001} , respectively, applied along the [100], [110], and [001] crystallographic directions [see methods in Supplemental Material (SM) Sec. A [23]]. Our unstressed samples display a single transition according to the specific heat. We report that the T_c value extracted from calorimetry decreases with compressive σ_{100} and σ_{110}

*cgirod@lanl.gov

†smthomas@lanl.gov

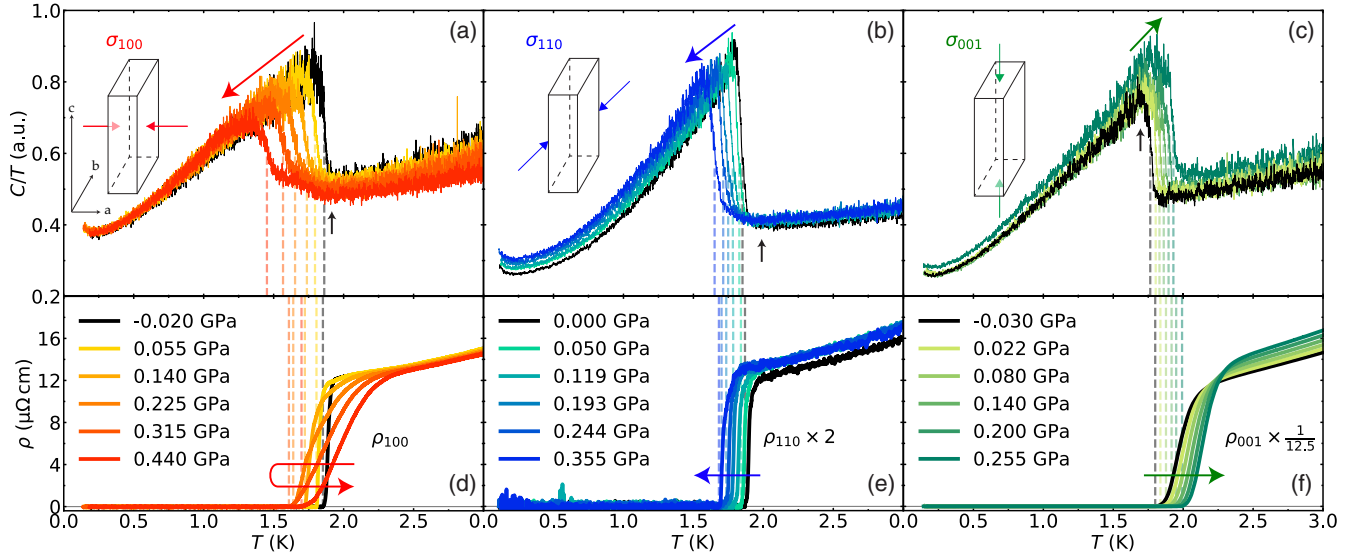


FIG. 1. Temperature dependence of the heat capacity C/T (top panels) and electrical resistivity (bottom panels) along the indicated crystal directions (ρ_{100} , ρ_{110} , and ρ_{001}) at the indicated uniaxial stress values and orientations [(a), (d) σ_{100} ; (b), (e) σ_{110} ; (c), (f) σ_{001}]. For each stress value, the dashed lines mark the average temperature of the sharp rise in C/T at $T_{c,ac}$ or the temperature $T_{c,\rho}$ below which ρ is zero. Colored arrows show the trends of $T_{c,ac}(\sigma)$ and $T_{c,\rho}(\sigma)$ upon increasing the compressive stress. Black arrows on the top panels show the onset [(a), (b)] and end [(c)] of the heat capacity jump of the lowest stress curve (black lines). The sketches show the direction of applied stress. ρ_{110} and ρ_{001} are scaled as indicated for clarity. The difference between the resistivity curves at the two lowest σ_{110} values is due to a crack in the sample, not to reversible piezoresistivity.

but increases with compressive σ_{001} . Most importantly, we show that a symmetry-breaking in-plane shear stress σ_{xy} does not induce any observable splitting of the superconducting transition. In addition, c -axis stress induces a significant piezoresistivity, presumably caused by the reduction of the energy scale corresponding to the feature observed at $T^* \approx 15$ K, attributed either to the onset of short-range magnetic correlations or anisotropic Kondo coherence [29–31].

Figures 1(a)–1(c) show the temperature dependence of the heat capacity plotted as C/T of three samples at the indicated σ_{100} , σ_{110} , and σ_{001} uniaxial stress values. In our convention, positive σ means compressive stress, whereas negative means tensile. The curves at the lowest stress show a single and sharp transition at the thermodynamic superconducting critical temperature $T_{c,ac}$, defined as the middle of the sharp rise in C/T that occurs when most of the sample becomes superconducting (dashed vertical lines). A single transition is in agreement with the characterization data of the unstressed samples (see SM Sec. A [23]) and with the results of Refs. [15, 16].

Figures 1(d)–1(f) show the temperature evolution of the electrical resistivity ρ with current along the applied stress direction. These measurements were carried out simultaneously with ac calorimetry. For ρ_{100} and ρ_{110} , the resistivity at the lowest stress value displays a sharp transition to the superconducting state at a resistive critical temperature $T_{c,\rho}$ (below which $\rho = 0$) that is in good agreement with the one extracted from heat capacity. For ρ_{001} , there is a slight difference between $T_{c,ac}$ and $T_{c,\rho}$ that may be related to the slower cooling rate that was used at the end of the sample growth (see Ref. [15]).

We observe two main effects upon application of compressive uniaxial stress. First, $T_{c,ac}$ changes monotonically upon applying stress along all directions. For σ_{100} and σ_{110} , $T_{c,ac}$

decreases with increasing stress, whereas $T_{c,ac}$ increases with increasing σ_{001} . The evolution of $T_{c,ac}$ and $T_{c,\rho}$ with σ_{100} , σ_{110} , and σ_{001} is summarized in the phase diagram shown in Fig. 2(a). As expected, the stress evolution of $T_{c,\rho}$ tracks that of $T_{c,ac}$ for most stress values. The difference between $T_{c,ac}$ and $T_{c,\rho}$ for $\sigma_{100} > 0.250$ GPa will be discussed later.

The opposite trend of $T_{c,ac}$ with σ_{100} (and σ_{110}) as compared to σ_{001} is in agreement with a previous thermal expansion study [32] that reported a negative jump at T_c in the linear thermal expansion coefficient along [100] (and [010]), but a positive jump for the coefficient along the [001] direction. This suggests that the superconducting state observed at ambient pressure is favored by a smaller c -axis length and larger a -axis length. Because the U-U dimer (shortest distance between U ions) in the crystal structure of UTe_2 is along the c axis, and uranium chains run along the a axis, our results support theoretical arguments that the c -axis dimer is key to the formation of the superconducting state in UTe_2 [33, 34].

The second effect of applied uniaxial stress is the appearance of a foot above $T_{c,ac}$ for σ_{100} and σ_{110} and a shoulder below $T_{c,ac}$ for σ_{001} [see Figs. 1(a) and 1(b), and Fig. 1(c), respectively]. As the number of superconducting transitions in UTe_2 remains a central question [13, 16], the origin of these features must be understood. It is clear from Figs. 1(a) and 1(b) that the foot above $T_{c,ac}$ for all σ_{100} and σ_{110} values coincides with the onset temperature of the superconducting anomaly of the lowest stress curve. For σ_{001} , the shoulder for all stress values extends above the temperature of the C/T jump at $T_{c,ac}$ of the lowest stress curve, as shown in Fig. 1(c). To demonstrate that these features are due to an inhomogeneous stress, especially in regions of the sample that extend underneath the mounting plates of the stress cell, we probed a smaller, more homogeneously stressed volume of the

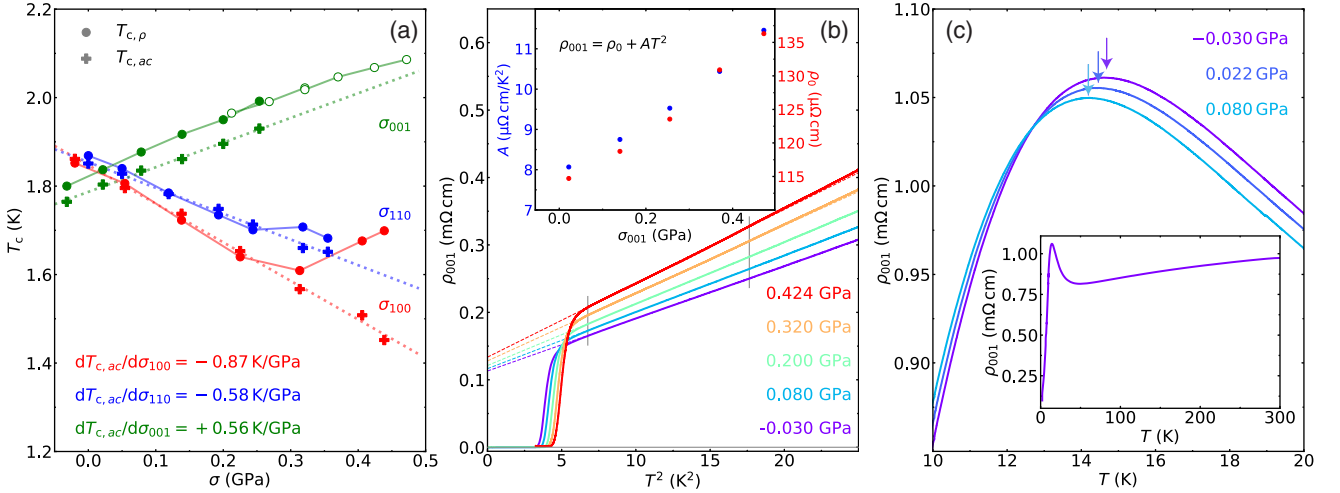


FIG. 2. (a) Superconducting transition temperatures $T_{c,\rho}$ (circles) and $T_{c,ac}$ (crosses) vs uniaxial stress. Solid symbols correspond to data from Fig. 1 and open symbols from (c) at higher σ_{001} values. Dashed lines are linear fits to $T_{c,ac}(\sigma)$. (b), (c) Temperature dependence of the c -axis resistivity ρ_{001} at different σ_{001} . (b) ρ_{001} below 5 K vs T^2 together with $\rho_{001} = \rho_0 + AT^2$ fits to the data between 2.6 and 4.2 K (dashed lines). The inset shows the σ_{001} dependence of ρ_0 and A . (c) Stress evolution of the peak at $T^* \approx 15$ K (colored arrows). The inset shows higher-temperature data at $\sigma_{001} = -0.030$ GPa.

samples by increasing the ac calorimetry excitation frequency [19]. The results for $\sigma_{100} = 0.050$ GPa and $\sigma_{001} = 0.200$ GPa are shown in SM Sec. B [23]. As expected when probing a more homogeneously stressed part of the sample, the position of the main heat capacity jump at $T_{c,ac}$ remains essentially unchanged while the shoulder and foot onset temperatures progressively merge with $T_{c,ac}$. This shows that stress inhomogeneity is responsible for these two artifacts and that there is a *single* heat capacity jump related to bulk superconductivity at the indicated stress levels. As pointed out in Ref. [16], the presence of two superconducting anomalies in some unstressed samples could be related to a lower sample quality.

Our main finding is the absence of splitting in the superconducting transition for σ_{100} , σ_{110} , and σ_{001} , as seen in Figs. 1(a)–1(c). This is especially meaningful for σ_{110} , which, unlike σ_{100} and σ_{001} , breaks the orthorhombic symmetry to monoclinic by lowering the point group symmetry from D_{2h} to C_{2h} . By expressing the [110] stress vector into the basis of the main crystallographic axes, one finds that it has components along [100] and [010] in addition to a pure shear stress contribution σ_{xy} in the ab plane whose amplitude is equal to $0.47\sigma_{110}$ (see details in SM Sec. A [23]). Because the resulting shear strain ϵ_{xy} transforms as the B_{1g} irrep of D_{2h} , it is expected to split the transition temperatures of the two proposed nearly degenerate OPs [13] because their product also transforms as B_{1g} . The temperature difference between the two nearly degenerate transitions ΔT_c is expected to follow (to leading order in the applied strain),

$$\Delta T_c = \sqrt{\Delta T_{c(\epsilon_{xy}=0)}^2 + \lambda^2 \epsilon_{xy}^2},$$

where $\Delta T_{c(\epsilon_{xy}=0)}$ is the unstressed splitting of the superconducting transition temperatures ($\Delta T_{c(\epsilon_{xy}=0)} \approx 0$ in our case) and λ is a coupling constant (see details in SM Sec. E [23]).

The absence of a detectable splitting in T_c upon application of σ_{110} [see Fig. 1(b)] may be explained by different

scenarios. One possibility is that the OP is different from the one proposed previously, either because there is only a single superconducting OP or because the nearly degenerate OPs belong to symmetry channels that would not allow for a coupling that is linear in ϵ_{xy} . Another possible explanation for the absence of detectable splitting of the superconducting transition induced by σ_{110} would be a λ value too small to cause any appreciable splitting for $\sigma_{110} < 0.355$ GPa. Using the elastic tensor obtained from density functional theory (DFT) (see SM Sec. D [23]), we find that at $\sigma_{110} = 0.355$ GPa, the induced $\epsilon_{xy} \approx -0.6\%$ would not lead to a ΔT_c greater than 0.1 K for $\lambda < 16$ K.

If UTe_2 hosts a single superconducting OP, regardless of its symmetry, one expects T_c to evolve quadratically with shear strain $T_c = T_c^{(\epsilon_{xy}=0)} + \lambda \epsilon_{xy}^2$. From Fig. 2(a), $T_{c,ac}$ evolves linearly with σ_{110} , which implies that the σ_{110} response is dominated by the symmetry-preserving stress components along [100] and [010] rather than the symmetry-breaking stress σ_{xy} . From symmetry arguments, T_c should be linear under applied symmetry-preserving stress.

From Fig. 2(a), we determine $\frac{dT_{c,ac}}{d\sigma_{100}} \approx -0.87$ K/GPa and $\frac{dT_{c,ac}}{d\sigma_{001}} \approx +0.56$ K/GPa, whose sum is -0.31 K/GPa. Upon comparison with both hydrostatic pressure studies [3,4] ($\frac{dT_c}{dP} \approx -0.5$ K/GPa) and thermal expansion and specific heat using Ehrenfest's relation [32] ($\frac{dT_c}{dP} \approx -0.49$ K/GPa), this result suggests that the evolution of T_c under applied compressive stress along [010] has a negative slope that is smaller than that of the two other axes. Using the elastic tensor calculated by DFT we find that the evolution of T_c with σ_{100} and σ_{001} cannot be explained in terms of strain along a single direction through Poisson effects. This suggests that there is no dominant strain direction controlling T_c in UTe_2 .

Under hydrostatic pressure, the superconducting transition splits into two above 0.3 GPa, leading to a slight slope change of the lower $T_c(P)$ and an initial enhancement of the higher $T_c(P)$. The latter undergoes a drastic suppression for

$P > 1.2$ GPa [3,4] due to the emergence of a magnetic ground state. Here, the absence of splitting of the superconducting transition and the linear evolution of $T_{c,ac}$ with uniaxial stress approaching 0.3 GPa (σ_{001}) or exceeding this value (σ_{100} and σ_{110}) suggests that higher stress levels would be required to drive the system to a regime with a different ground state. However, for $\sigma_{100} > 0.250$ GPa, $T_{c,\rho}$ starts to increase with increasing stress, in contrast to the behavior of $T_{c,ac}$ [see Fig. 2(a)]. In addition, the resistive superconducting transition shows substantial broadening upon application of σ_{100} whereas its width barely increases with σ_{110} and σ_{001} , as shown in Figs. 1(d)–1(f). This behavior was verified in another sample with applied σ_{100} (see SM Sec. C [23]).

For hydrostatic pressures above 0.3 GPa, the emerging superconducting transition that splits from the main $T_c(P)$ curve displays a positive dT_c/dP , an initially small signature in heat capacity, and a significant broadening in resistivity [3,4]. A similar scenario could thus take place under σ_{100} based on the analogous resistive behavior. In this case, a stress value of $\sigma_{100} \approx 0.3$ GPa could be just enough to drive the system towards the regime in which a split superconducting transition emerges. This would mean that a shorter U-U distance in the chains along the a axis could be a key ingredient for the enhancement of the second superconducting phase observed at high pressures. Alternatively, this effect may also be caused by the presence of filamentary or surface superconductivity. The application of higher stress will be useful to distinguish between the two scenarios.

Finally, we turn to the pronounced piezoresistivity observed above $T_{c,\rho}$ for stress and current along the c axis [see Fig. 1(f)], which was not observed for stress along other crystal directions [Figs. 1(d) and 1(e)]. By fitting the normal-state ρ_{001} over the temperature range shown in Fig. 2(b) to $\rho_{001} = \rho_0 + AT^2$, we observe an enhancement of both the coefficient associated with electron-electron scattering A and the residual resistivity ρ_0 upon increasing compressive σ_{001} . The observed enhancement of A over a stress range of about 0.5 GPa is significant (30%) but smaller than the factor of two increase in A with an applied hydrostatic pressure of 0.56 GPa [3] and much smaller than the $\sim 1000\%$ increase in A at a metamagnetic transition near 32 T for magnetic fields applied close to the b axis at atmospheric pressure [35]. These

comparisons suggest that at $\sigma_{001} \approx 0.5$ GPa, the system is still away from a hypothetical quantum critical point. It would be interesting to apply higher c -axis stress, which also seems to be tuning the system in a different direction than hydrostatic pressure [3,4]. Additionally, we find that the peak in ρ_{001} around $T^* \approx 15$ K that was previously reported in Ref. [31], shifts towards lower temperatures as σ_{001} increases, as displayed in Fig. 2(c). This peak has been attributed to either an anisotropic Kondo energy scale [30] or to the onset of short-range magnetic correlations [29].

In conclusion, our measurements under uniaxial stress show that the single bulk thermodynamic superconducting transition at $T_{c,ac}$ in UTe_2 has opposite evolution under applied compressive stress $\sigma_{100}, \sigma_{110}$ ($\frac{dT_{c,ac}}{d\sigma_{100}}, \frac{dT_{c,ac}}{d\sigma_{110}} < 0$) and σ_{001} ($\frac{dT_{c,ac}}{d\sigma_{001}} > 0$). This suggests that superconductivity in UTe_2 is favored by a smaller c -axis length and larger a -axis length. Notably, through the application of a symmetry-breaking shear stress σ_{xy} , we do not observe the expected T_c splitting for the case of two nearly degenerate superconducting OPs whose product transforms as B_{1g} . This implies either that the coupling between shear strain and the OPs is very small or that the superconducting OP of UTe_2 is different from the one proposed previously. In the latter scenario, TRS breaking might be explained by the condensation of a subleading superconducting instability near dislocations and other lattice defects, similarly to what has been recently proposed in Sr_2RuO_4 [36]. To disentangle these different scenarios, Kerr effect measurements are needed on crystals showing a single superconducting transition.

The LANL LDRD program supported the development of ac calorimetry under uniaxial stress. The remaining experimental work and crystal synthesis at LANL were supported by the U.S. DOE, Office of Basic Energy Sciences project “Quantum Fluctuations in Narrow Band Systems.” J.X.Z. (DFT calculations) was supported by the Quantum Science Center and in part by CINT, in partnership with the LANL Institutional Computing Program. C.S. and A.H. (crystal synthesis) were supported by U.K. EPSRC Grant No. EP/P013686/1. R.M.F. (phenomenological modeling) was supported by the U.S. DOE, Office of Basic Energy Sciences, Award No. DE-SC0020045.

-
- [1] S. Ran, C. Eckberg, Q.-P. Ding, Y. Furukawa, T. Metz, S. R. Saha, I.-L. Liu, M. Zic, H. Kim, J. Paglione, and N. P. Butch, *Science* **365**, 684 (2019).
- [2] D. Aoki, J.-P. Brison, J. Flouquet, K. Ishida, G. Knebel, Y. Tokunaga, and Y. Yanase, *J. Phys.: Condens. Matter* **34**, 243002 (2022).
- [3] D. Braithwaite, M. Vališka, G. Knebel, G. Lapertot, J.-P. Brison, A. Pourret, M. E. Zhitomirsky, J. Flouquet, F. Honda, and D. Aoki, *Commun. Phys.* **2**, 147 (2019).
- [4] S. M. Thomas, F. B. Santos, M. H. Christensen, T. Asaba, F. Ronning, J. D. Thompson, E. D. Bauer, R. M. Fernandes, G. Fabbri, and P. F. S. Rosa, *Sci. Adv.* **6**, eabc8709 (2020).
- [5] D. Aoki, F. Honda, G. Knebel, D. Braithwaite, A. Nakamura, D. Li, Y. Homma, Y. Shimizu, Y. J. Sato, J.-P. Brison, and J. Flouquet, *J. Phys. Soc. Jpn.* **89**, 053705 (2020).
- [6] S. Ran, H. Kim, I.-L. Liu, S. R. Saha, I. Hayes, T. Metz, Y. S. Eo, J. Paglione, and N. P. Butch, *Phys. Rev. B* **101**, 140503(R) (2020).
- [7] S. Ran, S. R. Saha, I.-L. Liu, D. Graf, J. Paglione, and N. P. Butch, *npj Quantum Mater.* **6**, 75 (2021).
- [8] S. Ran, I.-L. Liu, Y. S. Eo, D. J. Campbell, P. M. Neves, W. T. Fuhrman, S. R. Saha, C. Eckberg, H. Kim, D. Graf, F. Balakirev, J. Singleton, J. Paglione, and N. P. Butch, *Nat. Phys.* **15**, 1250 (2019).
- [9] G. Knebel, W. Knafo, A. Pourret, Q. Niu, M. Vališka, D. Braithwaite, G. Lapertot, M. Nardone, A. Zitouni, S. Mishra, I. Sheikin, G. Seyfarth, J.-P. Brison, D. Aoki, and J. Flouquet, *J. Phys. Soc. Jpn.* **88**, 063707 (2019).

- [10] L. Jiao, S. Howard, S. Ran, Z. Wang, J. O. Rodriguez, M. Sigrist, Z. Wang, N. P. Butch, and V. Madhavan, *Nature (London)* **579**, 523 (2020).
- [11] S. Bae, H. Kim, Y. S. Eo, S. Ran, I.-L. Liu, W. T. Fuhrman, J. Paglione, N. P. Butch, and S. M. Anlage, *Nat. Commun.* **12**, 2644 (2021).
- [12] T. Metz, S. Bae, S. Ran, I.-L. Liu, Y. S. Eo, W. T. Fuhrman, D. F. Agterberg, S. M. Anlage, N. P. Butch, and J. Paglione, *Phys. Rev. B* **100**, 220504(R) (2019).
- [13] I. M. Hayes, D. S. Wei, T. Metz, J. Zhang, Y. S. Eo, S. Ran, S. R. Saha, J. Collini, N. P. Butch, D. F. Agterberg, A. Kapitulnik, and J. Paglione, *Science* **373**, 797 (2021).
- [14] D. S. Wei, D. Saykin, O. Y. Miller, S. Ran, S. R. Saha, D. F. Agterberg, J. Schmalian, N. P. Butch, J. Paglione, and A. Kapitulnik, *Phys. Rev. B* **105**, 024521 (2022).
- [15] L. P. Cairns, C. R. Stevens, C. D. O'Neill, and A. Huxley, *J. Phys.: Condens. Matter* **32**, 415602 (2020).
- [16] P. F. S. Rosa, A. Weiland, S. S. Fender, B. L. Scott, F. Ronning, J. D. Thompson, E. D. Bauer, and S. M. Thomas, *Commun. Mater.* **3**, 33 (2022).
- [17] S. Sundar, S. Gheidi, K. Akintola, A. M. Côté, S. R. Dunsiger, S. Ran, N. P. Butch, S. R. Saha, J. Paglione, and J. E. Sonier, *Phys. Rev. B* **100**, 140502(R) (2019).
- [18] J. Ishizuka and Y. Yanase, *Phys. Rev. B* **103**, 094504 (2021).
- [19] Y.-S. Li, R. Borth, C. W. Hicks, A. P. Mackenzie, and M. Nicklas, *Rev. Sci. Instrum.* **91**, 103903 (2020).
- [20] V. Grinenko, S. Ghosh, R. Sarkar, J.-C. Orain, A. Nikitin, M. Elender, D. Das, Z. Guguchia, F. Brückner, M. E. Barber, J. Park, N. Kikugawa, D. A. Sokolov, J. S. Bobowski, T. Miyoshi, Y. Maeno, A. P. Mackenzie, H. Luetkens, C. W. Hicks, and H.-H. Klauss, *Nat. Phys.* **17**, 748 (2021).
- [21] K. Ishida, H. Mukuda, Y. Kitaoka, K. Asayama, Z. Q. Mao, Y. Mori, and Y. Maeno, *Nature (London)* **396**, 658 (1998).
- [22] A. Pustogow, Y. Luo, A. Chronister, Y.-S. Su, D. A. Sokolov, F. Jerzembeck, A. P. Mackenzie, C. W. Hicks, N. Kikugawa, S. Raghu, E. D. Bauer, and S. E. Brown, *Nature (London)* **574**, 72 (2019).
- [23] See Supplemental Material at <http://link.aps.org/supplemental/10.1103/PhysRevB.106.L121101> for additional details on sample preparation and characterization, experimental setup, as well as additional data, theoretical descriptions of the phenomenological model for the effect of shear strain, and DFT calculation of the elastic constants, which include Refs. [24–28].
- [24] G. Kresse and D. Joubert, *Phys. Rev. B* **59**, 1758 (1999).
- [25] G. Kresse and J. Furthmüller, *Phys. Rev. B* **54**, 11169 (1996).
- [26] G. Kresse and J. Hafner, *Phys. Rev. B* **48**, 13115 (1993).
- [27] A. I. Liechtenstein, V. I. Anisimov, and J. Zaanen, *Phys. Rev. B* **52**, R5467 (1995).
- [28] D. R. Boehme, M. C. Nichols, R. L. Snyder, and D. P. Matheis, *J. Alloys Compd.* **179**, 37 (1992).
- [29] K. Willa, F. Hardy, D. Aoki, D. Li, P. Wiecek, G. Lapertot, and C. Meingast, *Phys. Rev. B* **104**, 205107 (2021).
- [30] B. Kang, S. Choi, and H. Kim, *npj Quantum Mater.* **7**, 64 (2022).
- [31] Y. S. Eo, S. R. Saha, H. Kim, S. Ran, J. A. Horn, H. Hodovanets, J. Collini, W. T. Fuhrman, A. H. Nevidomskyy, N. P. Butch, M. S. Fuhrer, and J. Paglione, *Phys. Rev. B* **106**, L060505, (2022).
- [32] S. M. Thomas, C. Stevens, F. B. Santos, S. S. Fender, E. D. Bauer, F. Ronning, J. D. Thompson, A. Huxley, and P. F. S. Rosa, *Phys. Rev. B* **104**, 224501 (2021).
- [33] T. Shishidou, H. G. Suh, P. M. R. Brydon, M. Weinert, and D. F. Agterberg, *Phys. Rev. B* **103**, 104504 (2021).
- [34] L. Miao, S. Liu, Y. Xu, E. C. Kotta, C.-J. Kang, S. Ran, J. Paglione, G. Kotliar, N. P. Butch, J. D. Denlinger, and L. A. Wray, *Phys. Rev. Lett.* **124**, 076401 (2020).
- [35] W. Knafo, M. Nardone, M. Vališka, A. Zitouni, G. Lapertot, D. Aoki, G. Knebel, and D. Braithwaite, *Commun. Phys.* **4**, 40 (2021).
- [36] R. Willa, M. Hecker, R. M. Fernandes, and J. Schmalian, *Phys. Rev. B* **104**, 024511 (2021).